Reflexion of a plane wave onto a slope and wave-induced mean flow

Matthieu Leclair [1], Nicolas Grisouard[1,2], Louis Gostiaux [1], Chantal Staquet [1] and Francis Auclair [3]

[1] *Laboratoire des Ecoulements Géophysiques et Industriels, Grenoble, France*
[2] *Courant Institute of Mathematical Sciences, New-York, USA*
[3] *Pôle d'Océanographie Côtière, Laboratoire d'Aérologie, Toulouse, France*

Matthieu.Leclair@legi.grenoble-inp.fr

Abstract

Several processes lead to mixing and transport in the ocean, among those being the interaction of the internal gravity wave field with bottom topography. The latter process is considered in the present work, through joint laboratory experiments and numerical simulations. The laboratory experiments have been performed on the Coriolis platform in Grenoble and two- and three-dimensional numerical simulations have been carried out with the Symphonie-NH code. The basic configuration is a quasi-plane wave reflecting onto a simple slope in a uniformly stratified fluid. As expected, the interaction between the incident and reflected waves produces harmonic waves, thereby reducing the amplitude of the reflected wave. In the laboratory experiments however, the reflected wave is nearly absent because a wave-induced mean flow appears in the superposition region of the incident and reflected waves, which grows in amplitude. This mean flow is of dissipative origin and three-dimensional and its presence totally modifies the two-dimensional view considered in the literature.

Introduction

The processes and locations of mixing in the ocean have been the subject of an intense debate for more than fifteen years, when it was discovered from *in situ* measurements (Ledwell et al., 1993) that mixing in the interior of the ocean was ten times smaller than required from global balance arguments to maintain the thermal equilibrium of the ocean (Munk, 1966; Munk and Wunsch, 1998). The role of the boundaries in mixing processes was put forward to account for this 'missing mixing', as it was sometimes referred to, renewing past interest on that topic (f.i. Cacchione and Wunsch, 1974). Several boundary processes may indeed lead to mixing and transport processes, among those being the interaction of the internal gravity wave field with bottom topography. The latter process is considered in the present work.

A simple geometrical argument was proposed by Phillips (1966) for an internal wave impinging on topography, which leads to energy transfer to small scales. In a uniformly stratified medium, the dispersion relation of internal gravity waves is $\omega = N\sin\theta$, where ω is the wave frequency, N is the (constant) Brunt-Vaisala frequency of the medium and θ is the angle of the group velocity with the horizontal. Assuming the wave propagates in a medium at rest, the conservation of ω upon reflexion implies that the reflected wave is focused if $\theta \geq \alpha$, α being the local slope angle of the topography; namely the amplitude and wavenumber of the reflected wave increase near the boundary. For θ close to α, focusing leads to nonlinear processes (McPhee-Shaw and Kunze, 2002) and organized structures sometimes referred as bores (f.i. Hosegood and van Haren, 2004). This situation is referred to as critical incidence. For θ larger than α, the opportunity for nonlinear and transport processes is usually assumed to be rather rare. As Thorpe (1987) showed it theoretically, incident and reflected plane waves can form a resonant triad with a second harmonic wave resulting from the interaction of those

waves, opening the possibility of local increase of the amplitude away from the slope. In natural media however, internal gravity waves propagate as beams so that the possible occurence of resonance is limited to the interaction region between the incident and reflected beams. The occurence of such resonant interactions on a simple slope has been investigated numerically and experimentally in a quasi-two-dimensional vertical geometry by Rodenborn et al. (2011). One exception leading to transport properties when $\theta > \alpha$ is when the plane of the incident wave is not normal to the plane of the topography, assumed to be a simple slope. In this case indeed, a strong horizontal mean flow is observed leading to transport along the slope from the interaction region (f.i. Zikanov and Slinn, 2001).

The purpose of the present paper is to show that a mean flow actually appears even when the incident plane is normal to the slope, which is induced by the wave field. The conditions for this mean flow to exist are the fluid domain not to be two-dimensional and the incidence angle not to be critical.

The next section is devoted to a brief account on wave-induced mean flows. We present in Section 3 the two- and three-dimensional numerical and laboratory set-ups we used to study reflection on a simple slope. The energy sinks of the incident wave are discussed in Section 4; these are the reflected wave, harmonic waves resulting from the interaction between the incident and reflected waves, and a mean flow. Results between the laboratory experiments and the two-dimensional numerical simulations are also compared.

1 A brief account on wave-induced mean flow

It is well-known that waves, whether dispersive or not (such as surface gravity waves or sound waves), induce an irreversible mean flow if the waves propagate in a dissipative medium (see f.i. Lighthill, 1978). More precisely, as stated by the non-acceleration theorem, a linear steady wave propagating in a non-dissipative medium does not induce any mean flow (Andrews et al., 1987). It follows that, for a small-amplitude wave, either transient or dissipative effects accelerate the flow, thereby modifying the ambient mean flow if present or inducing a mean flow if the fluid is initially at rest. The mean flow response to wave transience is bounded in time and reversible, while the mean flow changes due to wave dissipation are cumulative in time and irreversible. This implies that mean motions induced by dissipative internal gravity waves can have a major effect on the flow, such as interacting with the waves themselves. The amplitude of the mean flow is proportional to the square of the wave amplitude, implying that wave-wave interactions are also a basic ingredient in mean flow generation (see (Bühler, 2009, p. 98)).

As is well-known, a dissipative mean flow results from momentum conservation : as the wave progresses forward, the wave-induced momentum flux decreases through molecular effects so that momentum is deposited by the wave as it propagates. This momentum deposit may be expressed as a force exerted on the fluid, which accelerates the fluid and produces the mean flow.

As usual in fluid mechanics, either an Eulerian or a Lagrangian point of view can be adopted to express the flow properties and so is also for averaging. Thus, an Eulerian mean flow means that, at a fixed position, the fluid motion averaged over a wave period is non zero. A Lagrangian mean flow is computed from the average over a wave period following the motion of a fluid particle. Note that the Lagrangian mean flow may vanish while the Eulerian mean flow does not. An example will be provided below.

2 Experimental and numerical setups

2.1 Experimental set-up

Experiments have been performed by Nicolas Grisouard and Louis Gostiaux on the Coriolis platform in Grenoble (Grisouard, 2010). As sketched in Figure 1, a key aspect of the experiments is the use of a wave generator designed to produce a (quasi-)plane wave and originally designed to facilitate comparison with theoretical predictions (Gostiaux et al., 2007). Also drawn in Figure 1 is the sloping boundary (frame a), which makes an angle of 10% ($\approx 5.71°$) with the horizontal. In the present study, the generator produces a beam with 4 wavelengths and the plane of this incident beam is normal to the sloping boundary. The tank is stably-stratified with brine and an initial constant stratification profile is imposed, with $N = 0.41\,\mathrm{rad}\cdot\mathrm{s}^{-1}$. The tank is non rotating.

Velocity measurements are inferred from Particle Image Velocimetry within a vertical laser sheet approximately located in the center of the incident beam; the vertical plane of this laser sheet is referred to as the (x,z) plane in Figure 1b.

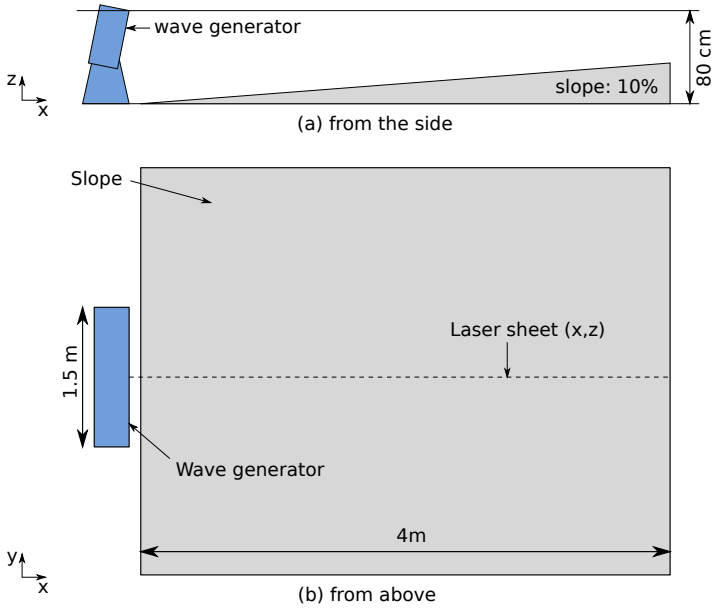

Figure 1: Sketch of the experimental set-up viewed from the side (a) and from above (b). The dashed line in frame (b) marks the vertical laser sheet where PIV measurements are performed.

2.2 Numerical set-up

Simulations have been carried out with the σ-coordinate non hydrostatic ocean model Symphonie-NH (Auclair et al., 2011).

Two-dimensional (x,z) simulations have first been performed. The code solves the non hydrostatic Boussinesq equations, with a linear equation of state. Horizontal boundary condition is a free surface at the top and is of free slip type at the bottom. The incident wave is produced thanks to a sponge layer at the left boundary where all variables (horizontal and vertical velocities and salinity anomaly) are restored towards the analytical plane wave solution modulated by an envelop in the z-direction. In order to avoid spurious reflections from the right boundary, another sponge layer is implemented where all variables are restored towards 0 at that boundary.

The resolution of the two-dimensional computations is $\Delta x \times \Delta z = 1\,\mathrm{cm} \times 0.5\,\mathrm{cm}$ along the x and z directions respectively. Simulations with a $\Delta x \times \Delta z = 2\,\mathrm{mm} \times 2\,\mathrm{mm}$ resolution have also been carried out, showing no important differences. For computational cost reasons, the first and coarser resolution has been retained. The diffusivity and viscosity are molecular and isotropic and respectively equal to $\kappa = 1.49 \times 10^{-9}\,\mathrm{m^2 s^{-1}}$ and $\nu = 10^{-6}\,\mathrm{m^2 s^{-1}}$ (the Prandtl number is therefore equal to 700).

Three-dimensional simulations have also been designed. The set-up in the vertical (x,z) plane is identical to the two-dimensional configuration. The internal wave forcing in the left sponge layer is limited in the y direction thanks to a smooth envelop. The resolution in the transverse direction is $\Delta y = 1\,\mathrm{cm} = \Delta x$. The viscosity and diffusivity values are unchanged compared to the 2D simulations.

3 Results

Experiments and numerical simulations have been performed using different forcing frequencies ω, and hence, from the dispersion relation, different angles θ of the incident wave field. In the present study, we focus upon the flow behavior obtained for $\omega = 42.16\,\mathrm{s}$, corresponding to $\theta = 18.6^\circ$. Both experiments and simulations have been run for 1000 s, that is about 24 wave periods, which was found to be large enough to reach a steady regime.

3.1 Incident and reflected waves

The incident and reflected waves are displayed in Figure 2 through the amplitude of the velocity field $|\mathbf{u}| = \sqrt{u^2 + w^2}$ times the sign of u to retain information on wave propagation; u and w are the x and z components of the velocity field respectively. Both experimental and (2D) numerical results are shown, with $\mathrm{sign}(u)\,|\mathbf{u}|$ being filtered at the forcing frequency over the last 8 wave periods .

This figure displays two main features. When compared with the experiment, the incident wave is remarkably reproduced by the numerical simulation, both in structure and amplitude. However, the reflected wave is nearly absent in the experiments, while it is still present, though rather weak, in the simulation. Also note the presence in both frames of an interference pattern where the incident and reflected waves superimpose.

3.2 Second harmonics waves

The same $|\mathbf{u}| = \sqrt{u^2 + w^2}$ field is plotted in Figure 3, now filtered at the second harmonics of the forcing frequency (2ω) over the last wave periods. A clear 2ω-wave has developed, whose maximum amplitude is about 10% of the primary wave amplitude. This wave results from the nonlinear interaction between the incident and reflected waves, as attested by its growing from the superposition region of these waves. In the simulation, the 2ω-wave has reflected on the free surface and on the sloping boundary. The same pattern is observed in the experiment but a reflected wave from the side of the Coriolis platform is also visible, which is absent in the simulation because of the sponge layer. Apart from a slight difference in amplitude between the experiment and the simulation (this amplitude is larger in the experiment), the main difference lies in the structure of the 2ω-wave: this wave is refracted near the topography in the experiment and, to a lesser extent, at the free surface too, while no such refraction is visible in the simulation. The refraction at the free surface is due to a thin mixed layer which develops in time from the surface. As for the bottom, another argument should be invoked, which is provided below.

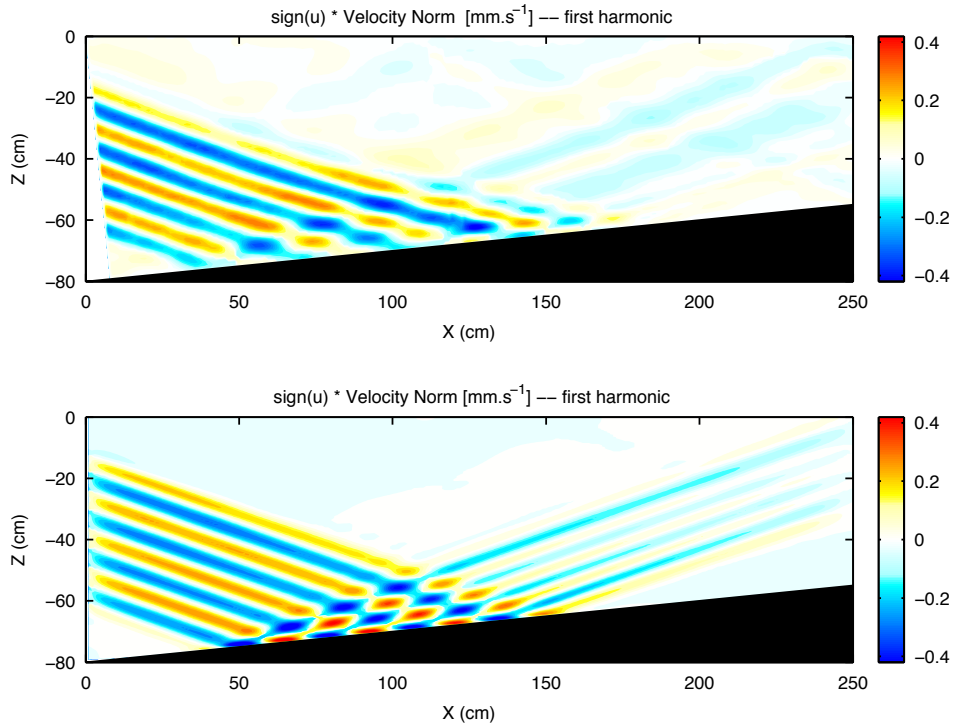

Figure 2: Comparison of experiments (top) and 2D simulations (bottom): first harmonic component. The field $\mathrm{sign}(u)\,|\mathbf{U}|$ is filtered over the last 8 wave periods at the fundamental (forcing) frequency and plotted in $\mathrm{mm}\cdot\mathrm{s}^{-1}$. The black triangle represents the sloping boundary.

3.3 Mean flow

The Eulerian mean flows computed for the experiment and the simulation are displayed in Figure 4. These mean flows strongly differ : in the simulation, the mean flow is an along-slope current which is periodic along the direction normal to the slope. This Eulerian mean flow has been predicted by Thorpe (1987) from a two-dimensional weakly nonlinear and inviscid analysis and is recovered here. In particular, its wavelength is equal to the difference in the reflected and incident wave vector components normal to the slope, which we checked. (As noted by Thorpe, the associated Lagrangian mean flow should be zero to account for the material conservation of density since the theory is inviscid.) We note that the amplitude of this mean flow is at most 10% of that of the incident wave, which is rather weak. The generation of this mean flow and, most importantly, of second and third harmonics (not shown) account for the weak amplitude of the reflected wave in the simulation.

In the experiment by contrast, a strong mean flow appears, which grows in time and reaches an amplitude comparable to that of the incident wave. Apart from a contribution due to the unsteadiness of the incident wave (before a -nearly- steady regime sets in), this mean flow is induced by wave dissipation. We checked that it is horizontal so that, because of the sloping boundary and the stable stratification, it must be three-dimensional. This accounts for its non existence in the two-dimensional numerical simulation. This also explains that the reflected wave is nearly absent in the experiment. As well, the refraction of the wave close to the boundary in Figure 3 can be explained from Doppler effect.

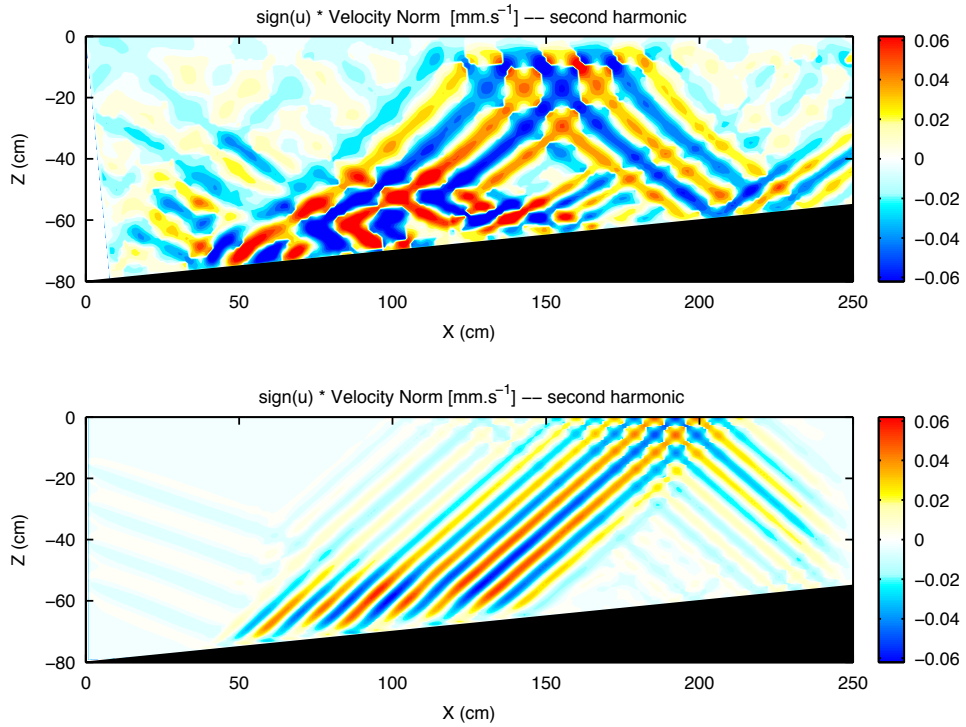

Figure 3: Comparison of experiments (top) and 2D simulations (bottom): second harmonic component. The field $\mathrm{sign}(u)\,|\mathbf{U}|$ is filtered over the last wave periods at frequency 2ω and plotted in $\mathrm{mm}\cdot\mathrm{s}^{-1}$. The black triangle represents the sloping boundary.

3.4 Preliminary three-dimensional numerical experiments

In order to study the characteristics of this mean current, ongoing three-dimensional simulations have been designed. The first results, after 130 s of simulation are illustrated on figure (5). The duration of the simulations is not long enough to apply the same harmonic analysis as for the 2D simulation and the experiment, so that only instantaneous fields are shown at this stage. Further analysis based on the complete 3D simulations will be presented at the conference.

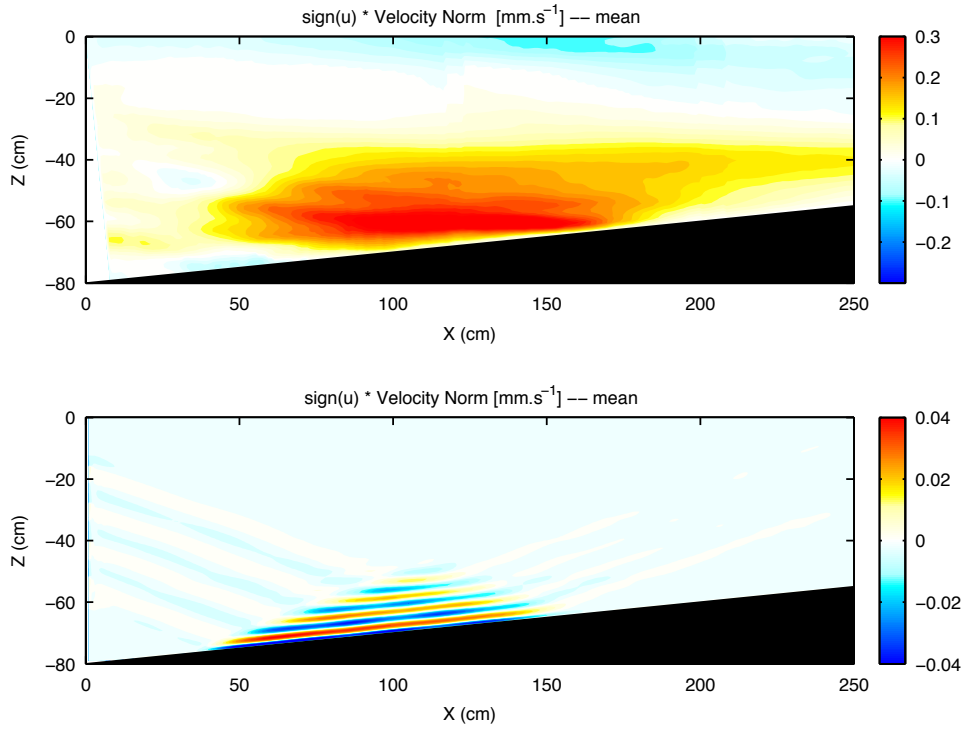

Figure 4: Comparison of experiments (top) and 2D simulations (bottom): mean component. The field $\text{sign}(u)\,|\mathbf{U}|$ is averaged over the last 8 wave periods. Note the difference in the color bars. The black triangle represents the sloping boundary.

References

Andrews, D., Holton, J., and Leovy, C. (1987). *Middle atmosphere dynamics*. Academic Press.

Auclair, F., Estournel, C., Floor, J. W., Herrmann, M., Nguyen, C., and Marsaleix, P. (2011). A non-hydrostatic algorithm for free-surface ocean modelling. *Ocean Modelling*, 36(1-2):49 – 70.

Bühler, O. (2009). *Waves and mean flows*. Cambridge University Press.

Cacchione, D. A. and Wunsch, C. (1974). Experimental study of internal waves over a slope. *J. Fluid Mech.*, 66:223–239.

Gostiaux, L., Didelle, H., Mercier, S., and Dauxois, T. (2007). A novel internal waves generator. *Experiments in Fluids*, 42:123–130. 10.1007/s00348-006-0225-7.

Grisouard, N. (2010). *Réflexions et réfractions non linéaires d'ondes internes de gravité*. PhD thesis (in French), University of Grenoble, France.

Hosegood, P. and van Haren, H. (2004). Near-bed solibores over the continental slope in the faroe-shetland channel. *Dear Sea Res. II*, 51:2943–2971.

Ledwell, J., Watson, A., and Law, C. (1993). Evidence for slow mixing across the pycnocline from an open-ocean tracer-release experiment. *Nature*, 364:701–703.

Lighthill, M. (1978). *Waves in Fluids*. Cambridge University Press.

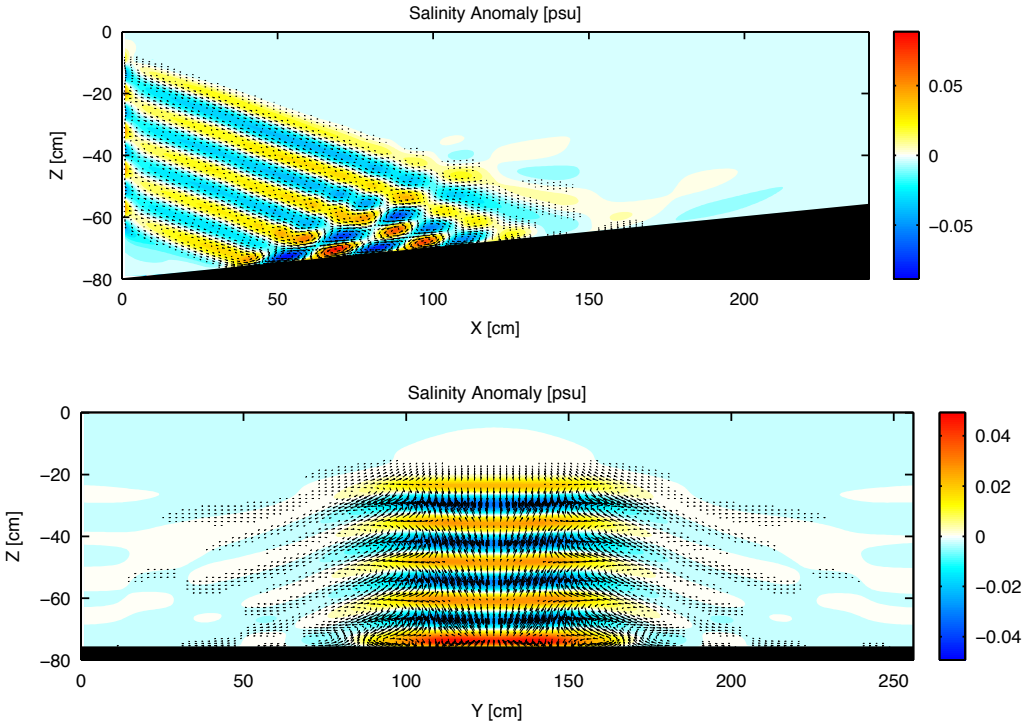

Figure 5: Ongoing 3D simulations. A (x,z) section in the middle of the domain (corresponding to the 2D figures) of the instantaneous salinity anomaly field after 130 s of simulation is plotted on the top frame. The same field is plotted in a (y,z) section at a distance $x = 40$ cm from the wave generator on the bottom frame. The velocity field is overplotted and represented with arrows. The black triangle (resp. rectangle) on the top (resp. bottom) panel represents the sloping boundary.

McPhee-Shaw, E. and Kunze, E. (2002). Boundary layer intrusions from a sloping bottom: a mechanism for generating intermediate nepheloid layers. *J. Geophys. Res.*, 107(C6):10.1029/2001JC000801.

Munk, W. (1966). Abyssal recipes. *Deep Sea Res.*, 13:707–730.

Munk, W. and Wunsch, C. (1998). Abyssal recipes ii: energetics of tidal and wind mixing. *Deep Sea Res.*, 45:1977–2010.

Phillips, O. (1966). *Dynamics of the upper ocean*. Cambridge University Press.

Rodenborn, B., Kiefer, D., Zhang, H., and Swinney, H. (2011). Harmonic generation by reflecting internal waves. *Physics of Fluids*, 23:026601.

Thorpe, S. A. (1987). On the reflection of a train of finite-amplitude internal waves from a uniform slope. *Journal of Fluid Mechanics*, 178:279–302.

Zikanov, O. and Slinn, D. (2001). Along-slope current generation by obliquely incident internal waves. *J. Fluid Mech.*, 445:235–261.